Tetraphenylthiophene-Functionalized Poly(N-isopropylacrylamide): Probing LCST with Aggregation-Induced Emission

Chung-Tin Lai, Rong-Hong Chien, Shiao-Wei Kuo, and Jin-Long Hong*

Department of Materials and Optoelectronic Science, National Sun Yat-Sen University, Kaohsiung 80424, Taiwan, Republic of China

S *Supporting Information*

ABSTRACT: A hydrophobic tetraphenylthiophene (TP) center with novel aggregation-induced emission (AIE) property was chemically linked to two poly(N-isoprppylacrylamide) (PNIPAM) chains to obtain thermoresponsive polymers to study the relationships between the lower critical solution transitions (LCSTs) and the AIE-operative fluorenscence (FL) emission. Three ethynyl-terminated PNIPAMs with different molecular weights were synthesized via controlled atom transfer radical polymerization (ATRP) using ethynyl-functionalized initiator. The PNIPAMs were then coupled with diazide-funtionalized TP (TPN$_3$) via click reaction to obtain the desired TP-embedded polymers of Px (x = 1, 2, and 3). All three polymers show AIE-property from their solution fluorescence behavior in THF/hexane mixtures. In the aqueous solution, the TP-center served as a fluorogenic probe that reveals the LCSTs of polymers and its relation to the degree of TP labeling in terms of polymer concentration. The thermoresponsiveness of Px was demonstrated by the complete emission quench when heated at temperatures above LCST. Dissociation of the TP aggregates above LCST is responsible for the emission quench, which was evaluated through the uses of transmittance measurement, dynamic light scattering, and ^{1}H NMR spectra.
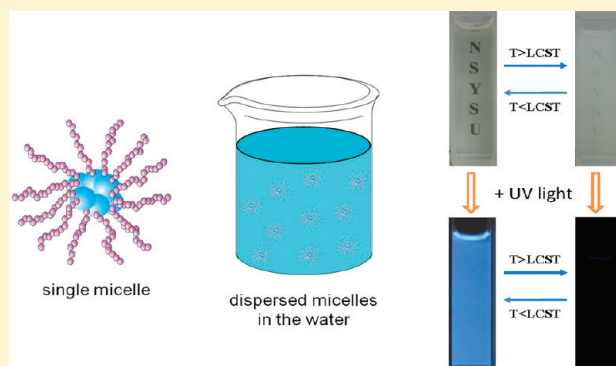
■ INTRODUCTION

Thermoresponsive water-soluble poly(N-isopropylacrylamide) (PNIPAM) in water displays a lower critical solution temperature (LCST), which has been investigated by a diversity of experimental techniques in the concentrated and dilute regimes.[1−12] Some possible models have been portrayed to account for the coil-to-globule collapse of PNIPAM in water.[13−15] The temperature-driven conformational transformation of the single PNIPAM chain and the macroscopic phase separation reflect rather subtle changes in polymer/water hydrogen-bonded interactions, primarily the release of water molecules from a polymer hydrophilic layer into bulk water. Therefore, slight changes in the chemical composition of PNIPAM are anticipated to have significant influences on the water/PNIPAM phase diagram.

Thanks to the Cerankowski and Taylor's efforts of scientists working in the LCST of poly(N-alkylacrylamides), such as PNIPAM, can be raised or lowered via introduction of hydrophilic or hydrophobic comonomers.[16] Since then, there have been numerous attempts to exploit this principle to create "intelligent" devices and systems capable to respond reliably and repetitively to temperature jumps.[17,18] One approach is the use of small number of long alkyl or perfluoroalkyl chains to generate hydrophobically modified (HM) PNIPAM.[19−23] The hydrophobic groups drive the self-assembly of the polymers, leading to the formation of polymeric micelles that exist as isolated entities in dilute cold aqueous solutions. Upon heating,

dehydration of the PNIPAM chains triggers changes in the size and shape of the micelles, often leading to macroscopic aggregation. The phase transition temperature depends not only on the level of hydrophobic incorporation and chemical structure but also on its position on the chain. This effect can be traced to differences in the structure of the micelles formed by the various HM-PNIPAMs in cold water. Randomly modified HM-PNIPAMs adopt a loose micellar conformation in which the hydrophobic groups are partly exposed to water; the cloud point of their solutions is depressed significantly compared to that of PNIPAM solutions.[24] On the other hand, polymers that carry a hydrophobic group at one chain end tend to form core−shell structures in which the hydrophobic core is insulated from the water by a brushlike corona of PNIPAM chains.[21,25] Like other associating polymers, such as hydrophobically modified ethoxylated urethanes (HEUR) or telechelic alkyl end-capped poly(ethylene oxides),[26−31] telechelic HM-PNIPAMs form flowerlike associates composing of loops of hydrated polymer chains and both end groups entrapped in the micellar core. In a preparatory dynamic light scattering measurement on the aqueous dilute solutions of telechelic C$_{18}$-PNIPAM-C$_{18}$, individual flower micelles collapse near LCST, forming colloidal state with an uneven segment density distribution.[29] Recently, Liu et al.,[30] Geckeler et al.[31] and

Scheme 1. Syntheses of Organic Compounds of TPBr, TPN₃, BMP, and the Click Reaction between PNIPAM*x* and TPN3 To Form P*x* Polymers
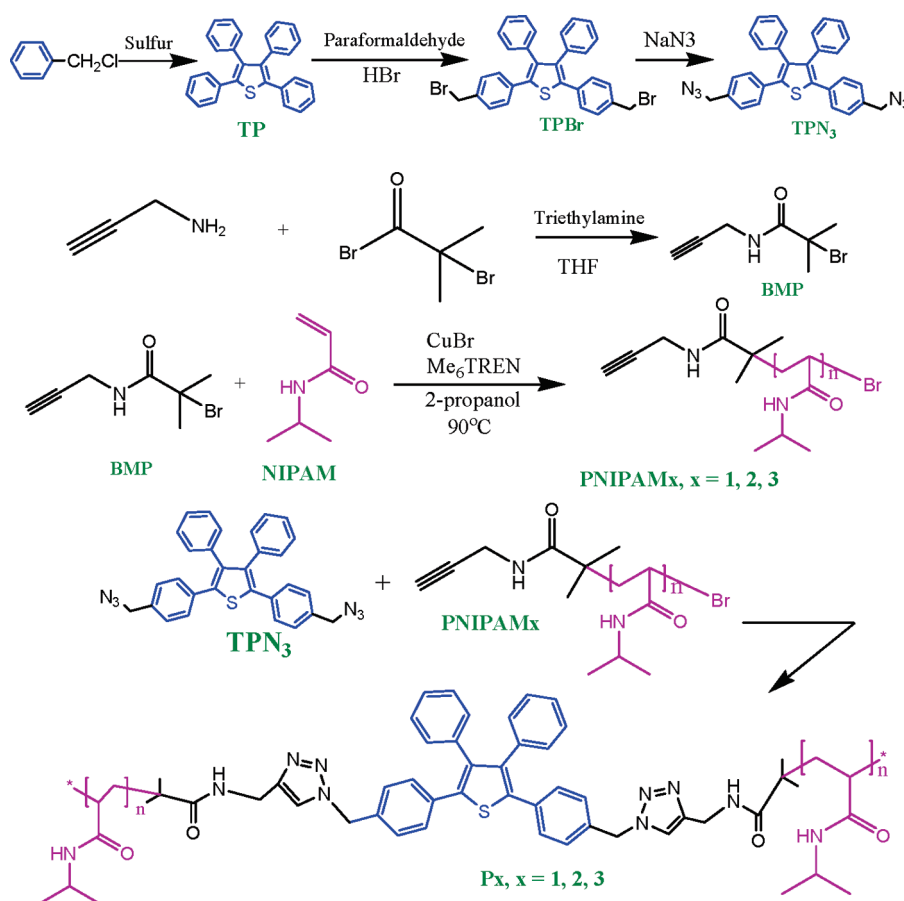
Yajima et al.[32] investigated the aggregation behavior of fullerene-(C₆₀-) functionalized PNIPAM (C₆₀-PNIPAM) in aqueous solution. The presence of highly hydrophobic C₆₀ moieties leads to self-assembled hybrid nanoparticles, which undergo thermo-induced collapse/aggregation behavior due to the LCST phase transition of PNIPAM chains.

In 2001, Tang's groups discovered that one particular silole molecule (1-methyl-1,2,3,4,5-pentaphenylsilole) emits strongly in the aggregated or the solid state even though it is nonemissive in the dilute solution.[33] This interesting phenomenon was designated as "aggregation-induced emission" (AIE) to emphasize the phenomenon that the originally nonluminescent solution of silole can be induced to emit strongly when the corresponding nanoaggregates formed after introduction of the poor solvent water. The AIE effect is rationalized as a result of restricted intramolecular rotation (IMR) of the phenyl peripheries against the central silole core in the aggregate state. Since the discovery of silole system, several AIE-active organic and polymeric materials[34–52] Recently, small amounts of AIE-active tetraphenylethene (TPE) comonomer were also incorporated into PNIPAM to study the emission response toward LCST.[45] The results indicated that when heated above LCST, varied FL emission responses were observed dependent on the degrees of TPE-labeling in the PNIPAM polymers.

We had previously studied on certain AIE-active systems,[50–52] among them, 2,3,4,5-tetra-phenylthiophene (TP, Scheme 1)

and its derivatives exhibit interesting properties. With the chemical framework of one central thiophene stator connected by multiple peripheral aromatic rings, TP and TP-derivatives were previously characterized to be AIE-active due to the restricted IMR. Compound TP and its derivatives can be readily prepared in high yields through facile electrophilic substitutions[51] (such as bromination, acetylation, nitration, ..., etc.). With the chemical readiness and the flexibility to prepare TP-derivatives, we thus prepared the well-defined thermoresponsive PNIPAM with AIE-active TP center (as P*x*, *x* = 1, 2 and 31) via the combination of atom transfer radical polymerization (ATRP) and click chemistry. We determined the temperature that triggers the coil-to-globule collapse of the main chain and the following aggregation and the thermodynamic values associated with the conformation change during the LCST transition. DLS, TEM, and temperature-dependent optical transmittance were employed to characterize the thermodynamic values associated with the conformational changes.

■ EXPERIMENTAL SECTION

Materials. Reagent grade benzyl chloride, sulfur powder, paraformaldehyde, hydrogen bromide solution (33% HBr solution in acetic acid), sodium azide, propargylamine, α-bromoisobutyryl bromide, triethyl amine, formic acid, tris(2-aminoethyl)amine, sodium hydroxide, dichloromethane (DCM), magnesium sulfate and 2-propanol were

purchased from Aldrich Chemical Co. and used directly without further purification. CuBr (98%, Aldrich) was stirred overnight in acetic acid, filtered and washed with ethanol and diethyl ether before dried in vacuo. *N*-Isopropylacrylamide (NIPAM) was purchased from Acros and recrystallized from hexane. THF was refluxed over sodium/benzophenone under nitrogen for more than 2−3 days before distillation to use. *N,N*-Dimethylformamide (DMF) was refluxed over CaH_2 under nitrogen for 5 h before distillation for use.

Syntheses of small molecules and polymer. Compound TP[53−55] and tris(2-dimethylaminoethyl)amine (Me_6-TREN)[56] were prepared by the reported procedures. Other organic molecules and polymers shown in Scheme 1 were prepared according to the detailed procedures given below.

Preparation of 2-(4-Nitrophenyl)-3,4,5-triphenylthiophene (TPBr). A mixture of TP (2 g, 5.15 mmol), paraformaldehyde (0.33 g, 11.0 mmol) and hydrogen bromide solution (33% HBr solution in acetic acid, 25 mL) was heated and reacted at 90 °C for 36 h. After cooling to room temperature, the precipitates were filtered, washed with water, and dried in vacuo to afford pale white yellow solid. Final product (2.16 g, 73%) was obtained by recrystallization from toluene/hexane. Mp: 215 °C. IR (KBr pellet, cm^{-1}): 3052, 3024, 2957, 2924, 2852, 1600, 1539, 1479, 1440, 1406, 1224, 1071, 1010, 825, 770, 701, 608 (Figure S4, Supporting Information). ^{1}H NMR (500 MHz, $CDCl_3$): δ 6.77−7.21 (m, 18H, aromatic *H*s), 4.36 (s, 4H, −C*H*$_2$Br) (Figure S1, Supporting Information): MS, *m/e*: calcd for $C_{30}H_{22}Br_2S$, 571.98; found, 572.03 (M^+). Anal. Calcd for $C_{30}H_{22}Br_2S$: C, 62.73; H, 3.86; Br, 27.82; S, 5.58. Found: C, 62.54; H, 4.05; S, 5.67.

Preparation of 3-Phenyl-5-(3,4,5-triphenylthiophen-2-yl)benzo[c]-isoxazole (TPN$_3$). Suspension of TPBr (1 g, 1.74 mmol) and sodium azide (1.13 g, 17.4 mmol) in DMF (20 mL) was heated at 80 °C for 48 h. Solvent was then removed from the reaction mixtures by vacuum distillation at elevated temperature. The resultant solid was redissolved in 30 mL dichloromethane and washed with 150 mL of saturated aq. NaCl solution twice. The organic layer was then dried over $MgSO_4$ and concentrated to obtain 0.8 g of TPN$_3$ (0.8 g, 92%) Mp: 229 °C. IR (KBr pellet, cm^{-1}): 3053, 3024, 2921, 2852, 2096, 1700, 1600, 1481, 1441, 1409, 1343, 1247, 1071, 820, 702 (Figure S4, Supporting Information). ^{1}H NMR (500 MHz, $CDCl_3$): δ 6.88−7.33 (m, 18H, aromatic *H*s), 4.27 (s, 4H, −C*H*$_2$N$_3$) (Figure S2, Supporting Information). MS, *m/e*: calcd for $C_{30}H_{22}N_6S$, 498.16; found, 498.12 (M^+). Anal. Calcd for $C_{30}H_{22}N_6S$: C, 72.27; H, 4.45; N, 16.86; S, 6.43. Found: C, 72.04; H, 5.22; N, 16.52; S, 6.21.

Preparation of Propargyl 2-Bromo-2-methylpropionamide (BMP). To an argon-blanketed solution of propargylamine (6.00 g, 5.45 mmol) and triethylamine (11.4 mL, 8.18 mmol) in THF (300 mL) at ice−water temperature, α-bromoisobutyryl bromide (12.5 g, 5.45 mmol) was slowly added. The reaction mixtures were warmed to room temperature and stirred overnight. The precipitate was filtered off and the solvent was removed by vacuum distillation. The crude product was purified through column chromatography (*n*-hexane/EtOAc, 4:1) to give **I** as a pale yellow solid (7.84 g, 70.5%). Mp: 52 °C. IR (KBr pellet, cm^{-1}): 3332, 3273, 3053, 2980, 2932, 2119, 1646, 1530, 1425, 1374, 1356, 1301, 1266, 1195, 1110, 1060, 1008, 910, 823, 697, 624, 581 (Figure S5, Supporting Information). ^{1}H NMR (500 MHz, $CDCl_3$): δ 6.88 (broad, 1H, N*H*), 4.05 (dd, 2H, CC*H*$_2$NH), 2.27 (t, 1H, C*H*≡C), 1.98 (s, 6H, C-(C*H*$_3$)$_2$Br) (Figure S3, Supporting Information). MS, *m/e*: calcd for $C_7H_{10}BrNO$, 202.99; found, 202.46 (M^+). Anal. Calcd for $C_7H_{10}BrNO$: C, 41.20; H, 4.94; Br, 39.16; N, 6.86; O, 7.84. Found: C, 40.98; H, 5.56; N, 6.59; O, 7.57.

Preparation of PNIPAM from ATRP. A 100 mL dried Schlenk flask containing a magnetic stirrer bar was charged with CuBr (14.3 mg, 0.1 mmol) and NIPAM (1.35 g, 10.6 mmol). After filling the flask with argon, 2-propanol (10 mL) was added and the solution was stirred for another 10 min at room temperature. The mixture was degassed three

Table 1. Click Reaction Results

polymer	n^a	n^b	M_w (g/mol)^c	M_n (g/mol)^c (n)^d	PDI^c
PNIPAM1	19		2900	2600 (20)	1.11
PNIPAM1	43		6000	5400 (41)	1.12
PNIPAM1	88		12800	11200 (86)	1.14
P1	38	42	5900	5300 (40)	1.11
P2	85	89	12100	10700 (83)	1.13
P3	175	181	25500	22600 (174)	1.13

^{a} Degree of polymerization calculated from the corresponding ^{1}H NMR (Figure 2). ^{b} Degree of polymerization calculated from the calibration curve (Figure S7). ^{c} Determined by GPC (Figure 1); based on polystyrene standard. ^{d} Degree of polymerization calculated from M_n (GPC analysis).

times using the freeze−pump−thaw cycle before vigorously stirred at 0 °C. After complete degassing, Me_6TREN (23.0 mg; 0.1 mmol) was injected into the solution via syringe. After 10 min, propargyl 2-bromo-2-methylpropionamide (BMP; for PNIPAM1, 0.11 g (0.54 mmol); for PNIPAM2, 55.1 mg (0.27 mmol); for PNIPAM3, 27.55 mg (0.135 mmol)) was injected into the solution to initiate the reaction. The mixture was at 0 °C for 48 h and then evaporated to dryness under vacuum. The residue was diluted with tetrahydrofuran (THF) and then passed through an alumina column to remove the copper catalyst. The product was precipitated from diethyl ether three times and dried under vacuum overnight at room temperature to obtain the polymer as a white powder (PNIPAM1, 1.2 g, 89.6%). PNIPAM1: T_g = 108 °C (Figure S6, Supporting Information); IR (KBr pellet, cm^{-1}) 3447, 3297, 3083, 2974, 2935, 2877, 2134, 1650, 1547, 1459, 1389, 1367, 1171, 1131; ^{1}H NMR (500 MHz, $CDCl_3$) δ 6.11−6.87 (broad, 2H, N*H*CO), 3.97 (broad, 1H, C*H*(CH$_3$)$_2$), 1.4−2.2 (broad, 3H, backbone *H*s), 1.18 (broad, 6H, CH(C*H*$_3$)$_2$).

Preparation of Px (Click Reaction). A typical procedure for the click reaction is as follows: DMF (15 mL) was placed in a three-neck flask and degassed by bubbling argon for 1 h before the addition of CuBr (20 mg, 0.14 mmol), TPN$_3$ (0.29 g, 0.59 mmol) and PNIPAM1 (0.15 g, 1.17 mmol). A solution of Me_6TREN (46 mg; 0.2 mmol) in degassed DMF (5 mL) was then introduced and the resultant transparent solution was then heated at 80 °C under in argon atmosphere for 33 h. When the mixture was cooled to room temperature, DMF was distilled off under reduced pressure. The residue was diluted with tetrahydrofuran (THF) and then passed through an alumina column to remove the copper catalyst. The solid product was then precipitated from diethyl ether. Further dissolution/precipitation procedures by THF/twice was repeated twice before vacuum drying to yield the final polymer as yellow powder (P1, 1.23 g, 75%). P1: T_g = 138 °C (Figure S6, Supporting Information); IR (KBr pellet, cm^{-1}) 3447, 3297, 3083, 2974, 2935, 2877, 1650, 1547, 1459, 1389, 1367, 1171, 1131 (Figure S5, Supporting Information); ^{1}H NMR (500 MHz, CD_2Cl_2) δ 6.97−7.36 (broad, aromatic *H*s), 6.11−6.87 (broad, N*H*CO), 3.97 (broad, C*H*(CH$_3$)$_2$), 1.4−2.2 (broad, backbone *H*s), 1.18 (broad, CH(C*H*$_3$)$_2$) (Figure 2). The synthesis of P2 and P3 followed the same procedures as those described for P1. The molecular parameters of the resultant polymers are summarized in Table 1.

Characterization. ^{1}H NMR spectra were recorded at various temperatures on a Varian VXR-500 MHz instrument (resonance frequency of 500 MHz) operated in the Fourier transform mode with CD_2Cl_2, or $CDCl_3$/D_2O as the solvent. A VG Quattro GC/MS/MS/DS instrument was used to determine the molar mass of the organic molecules. The sample was charged into the rapidly moving gas and converted into the corresponding ions, which were further separated based on their mass-to-charge ratios (*m/z*). Molecular weight and molecular weight distribution of polymers were determined from GPC using
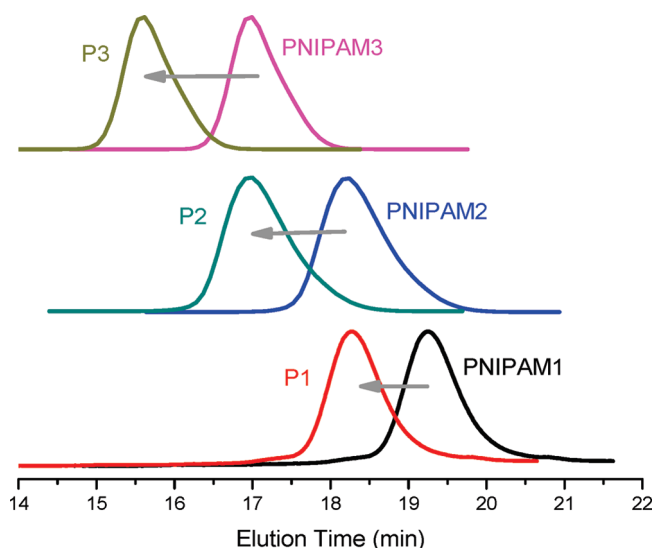
Figure 1. GPC elution curves of PNIPAM1, PNIPAM2, PNIPAM3, P1, P2, and P3 (RI detector).

Figure 2. ^{1}H NMR spectra of P1, P2, and P3 (CD$_2$Cl$_2$).

a Waters 510 HPLC model equipped with a 410 differential refractometer, a UV detector, and three Ultrastyragel columns (100, 500, and 1000 Å) connected in series. Polymer solution was eluted by THF with a flow rate of 0.6 mL/min. A set of monodisperse polystyrene standards covering molecular weight range of $10^3 – 10^6$ g/mol was used for the molecular weight calibration. The melting point (Mp) of the organic molecules and the glass transition temperatures (T_g) of the polymers were obtained from a TA Q-20 DSC calorimeter with a scan rate of 20 °C/min. FT-IR spectra were obtained on a Nicolet IR-200 spectrometer. Sample solution in THF was dropped on a KBr pellet and dried at 100 °C under vacuum to prepare the solid film for FT-IR analysis. UV–vis absorption and transmission spectra were recorded with an Ocean Optics DT 1000 CE 376 spectrophotometer. The temperature-variable experiment was carried out in a quartz cell with 1 cm ×1 cm dimension after the solution was left at the preset temperature for 30 min and the temperature was change with a step width of 1 °C. Temperature was controlled by an HCS 302 hot-stage, upon which a Peltier cell from OceanOptics was mounted.

Fluorescence (FL) emission spectra were obtained from a LabGuide X350 fluorescence spectrophotometer using a 450W Xe lamp as the continuous light source and a temperature controller. Fluorescence quantum yields (Φ_f) of the polymer solutions (1 mg/mL) in solvent mixtures of varied compositions were determined by comparison with a quinine sulfate standard (10^{-5} M in 0.1 N H$_2$SO$_4$, $\Phi_f = 0.55$). Particle sizes of polymer aggregates in solution were measured by dynamic light scattering (DLS) using a Brookhaven 90 plus spectrometer equipped with a temperature controller. An argon ion laser operating at 658 nm was used as light source. Cryo-transmission electron microscopy (cryo-TEM) was used to determine the size of the polymer nanoparticles. Samples were prepared according to protocols reported elsewhere[57,58] on a JEOL JEM-2100 LaB$_6$ microscope (Cs = 2.0 mm) operating at 200 kV. Digital images were recorded on a Gatan Ultrascan 1000 CCD camera.

■ RESULTS AND DISCUSSION

Synthesis of TP-Embedded Water-Soluble Homopolymers (P1, P2, and P3). As illustrated in Scheme 1, the highly efficient click reaction[59,60] between TPN$_3$ and PNIPAMx was used for the construction of TP-embedded polymers of P1, P2, and P3. The diazide-based organic compound of TPN$_3$ was prepared from the TP[53−55] compound through the two-step
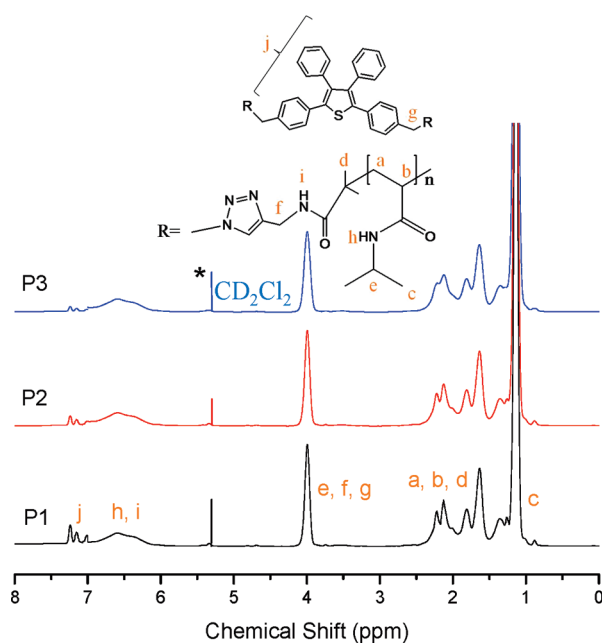
reaction procedure including bromomethylation of TP to obtain TPBr and the following diazidation of TPBr to obtain the desired diazide compound TPN$_3$. On the other hand, the alkynyl-terminated PNIPAMx polymers were prepared from ATRP of NIPAM monomer by an alkynyl-functionalized initiator of propargyl 2-bromo-2-methylpropionamide (BMP), which was synthesized from the reaction of propargyl amine and 2-bromo-2-methylpropanoyl bromide. Altogether, three polymers of PNIPAMx ($x = 1−3$) with different molecular weights were used in this study to proceed click reaction with TPN$_3$ to result in thermoresponsive homopolymers of P1, P2 and P3 with two hydrophilic PNIPAM chains linked to the same hydrophobic TP-center.

Chemical structures of all reaction intermediates were confirmed from the ^{1}H NMR, FTIR spectra (Figure S1−S5, Supporting Information) and the elemental analysis (included in Experimental Section). Infrared spectra can be primarily used to demonstrate the success of click reaction: the characteristic azide −N$_3$ absorption of TPN$_3$ and the ethynyl −C≡C band of PNIPAM1 are completely absent in the spectra of P1 (Figure S5, Supporting Information). The molecular weight increases from PNIPAMx to Px were also demonstrated from the corresponding GPC traces in Figure 1. Here, we observed that all Px polymers eluted at earlier time as compared to their respective PNIPAMx precursors. The degree of polymerization (n) calculated from the number-average molecular weight (M_n) is listed in Table 1, which suggests the well correlations between PNIPAMx and Px. The molecular weights can be also evaluated from the corresponding ^{1}H NMR spectra in Figure 2. The integration ratios between the proton H$_e$ (−CH(CH$_3$)$_2$)) and the aromatic protons can be used to formulate n values of P1, P2, and P3. The results in Table 1 suggest that n values of Px calculated from the ^{1}H NMR spectra are close to the ones evaluated from M_n, which indicated the successful TP-labeling via the efficient click reaction. According to the DSC thermograms (Figure S6, Supporting Information), glass transition temperatures (T_gs) of the PNIPAMx and Px polymers are in the range 108−144 °C, dependent on the molecular weights.
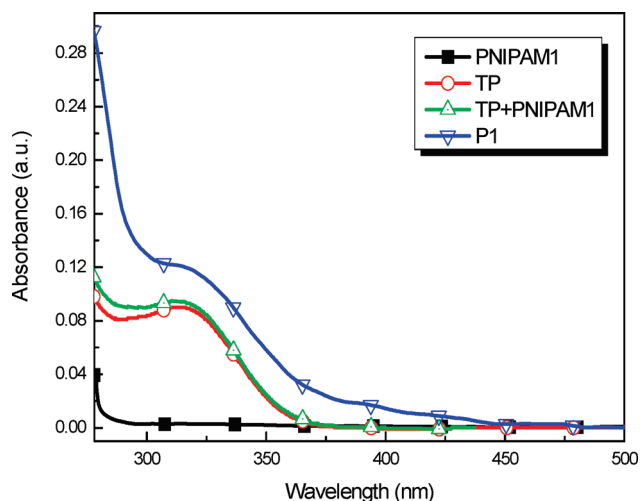
Figure 3. Absorption spectra of THF solutions of PNIPAM1 (1 mg/mL), TP (10^{-5} M), TP (10^{-5} M) in PNIPAM1 (1 mg/mL), and P1 (1 mg/mL) measured at 25 °C.

The presence of TP moiety in P1, P2, and P3 can be further verified from the UV–vis spectroscopy. Absorption spectrum of TP compound included in Figure 3 was used as standard to characterize the absorption spectrum of P1 polymer. Small molecule of TP in THF exhibits the characteristic absorption peak at 320 nm, which is essentially absent in the absorption spectrum of PNIPAM1. With the presence of TP fluorophore, P1 exhibits the same absorption band as mixtures of TP and PNIPAM do. The calibration curve (Figure S7, Supporting Information) based on the UV–vis absorption data of TP molecule in THF can be used to determine the degrees of TP labeling in P1, P2, and P3. According to Beer–Lambert law, the molar absorption coefficient (ε) from the calibration curve is 0.0927 L/mol × cm. The TP content in μmol/g of polymer can be determined by dividing the absorption of a polymer solution of known concentration in g/L by the molar absorption coefficient of TP in L/mol × cm. The TP content of the polymer can then be easily converted into a degree of polymerization. In consistent with the order of the molecular weight of the applied PNIPAM*x*, the degrees of TP labeling in P1, P2, and P3 are 2.33, 1.11, and 0.55%, respectively. As illustrated in Table 1, the resultant *n* values based on the UV–vis absorption spectra are well correlated with those from the ^{1}H NMR spectra and GPC, too.

AIE Effect. The AIE-active TP center facilitate the fluorescence of the P*x* polymers in the solution aggregated state. By adding poor solvent (hexane) to solution of P1 in good solvent (THF), the polymer aggregates formed should have stronger emission intensity if AIE effect comes into operation. Beforehand, solutions of P1 in THF/hexane mixtures were vigorously stirred to ensure uniform dispersion of the aggregates thus formed upon hexane inclusion. All the resultant mixture solutions (1 mg/mL) are macroscopically homogeneous but visually opaque, indicating the presence of nanoaggregate in the solvent mixtures. The resultant nanoaggregates are quite stable in the solvent mixtures without visible mass precipitations after standing for at least one month. Formations of nanoparticles can be confirmed by the particle size measurements from DLS (Figure S8, Supporting Information). No signal is recorded from the polymer solution in pure THF, indicating that polymer P1 is genuinely dissolved in the good solvent of THF. On the contrary,

polymer aggregates with the average diameters of 175–265 nm were detected in the THF/hexane mixtures with various hexane contents.

The solution FL emission spectra in Figure 4A clearly demonstrate the operative AIE properties of P1. Upon excitation at 320 nm, solution (1 mg/mL) of P1 in pure THF emitted weakly but with the gradual hexane inclusion in the THF/hexane solvent mixtures, the resultant solutions significantly developed their emission intensities. For the 90 vol % hexane solution, more than 83-fold intensity gain was achieved when compared to P1 in pure THF. In this case, the single fluorescent TP center in each of the polymer chain is supposed to associate with other TP fluorophores intermolecularly in order to exert the enhanced emission in the aggregated domains. The solution FL emission spectra of P2 and P3 in THF/hexane mixtures also confirmed the existence of AIE effect in these two polymers.

The solution fluorescent quantum yields (Φ_f) of P1, P2, and P3 solutions in THF/hexane mixtures were then measured and summarized in Figure 4B. Solutions of P1 with low hexane (<60 vol %) content have low Φ_fs (~0.0012) but beyond that, Φ_fs increase abruptly to reach a final value of 0.23 for the 90 vol %-hexane solution, which is ~190 times of that for P1 in pure THF. The lower degree of TP-labeling in P2 and P3 resulted in the lower Φ_f values in comparison to P1 solution; nevertheless, similar emission enhancements were observed for both when hexane content in the solutions is over 60 vol %. Under UV-light illumination, solutions of P1 in THF/hexane mixtures showed the progressive development on the fluorescence with the increasing hexane content in the solution (Figure 4C).

Self-Assembly of TP-Embedded Water-Soluble Homopolymers (P1, P2, and P3) in Aqueous Solution. On the basis of chemical intuition, TP-functionalized PNIPAM should self-assemble into micellar structures (Scheme 2) consisting of hydrophobic TP cores surrounded by the hydrophilic PNIPAM coronas in the dilute aqueous solution at room temperature. The intimate associations of TP fluorophores in the core domain should enhance the aggregation of the TP fluorophores and in this case, the FL emission intensity can be alternatively promoted due to the AIE-operative emission. Relationship between the FL emission behavior and the self-assembled morphology is therefore evaluated below.

Self-assembly behavior of TP-functionalized PNIPAMs in water was then investigated through their FL emission behavior. Primarily, it is safe to say that the FL emissions resolved for all P*x* polymers (Figure 5A) are due to the inherent TP unit since no FL emission can be detected for the aqueous PNIPAM1 solution. The FL emission spectra of P1, P2, and P3 in water all resemble to those obtained in the THF/hexane mixtures (Figure 4A) and consist of one broad emission centered at 405 nm. The emission intensity shown in Figure 5A is in the order of P1 > P2 > P3 and is therefore in line with the degree of TP-labeling in P*x*. The maximum peak intensities at 405 nm from other concentration ranges were monitored and were summarized in Figure 5B, which shows the trend of increasing emission intensity with the increasing polymer concentration for all three polymer solutions. Aggregations of the AIE-active TP fluorophores in the micelles are supposed to develop with increasing polymer concentration, leading to the enhanced emissions at higher concentrations. Primary evaluation in Figure 5B indicates that the peak intensity is proportional to the concentration of P*x* in water. In addition, the three traces in Figure 5B merge into a single linear curve in Figure 5C if intensity was plotted against the
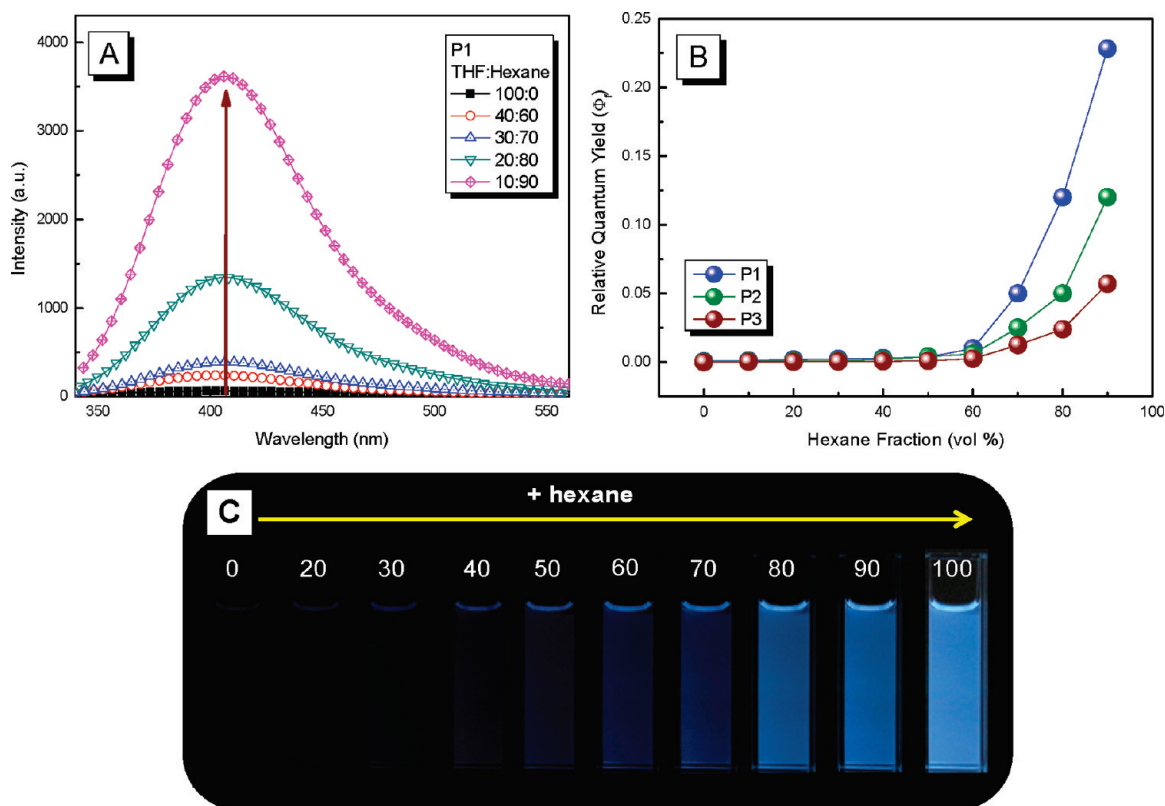
Figure 4. (A) FL emission spectra of P1 (1 mg/mL) in THF/hexane mixtures with different hexane contents (measured at 25 °C and λ_{ex} = 320 nm), (B) the relative quantum yields of Px in THF/hexane mixtures, and (C) photographs of P1 (1 mg/mL) in THF/hexane mixtures.

Scheme 2. Schematic Representation of the Core—Shell Micellar Structure of the TP-Embedded PNIPAM in Aqueous Solution
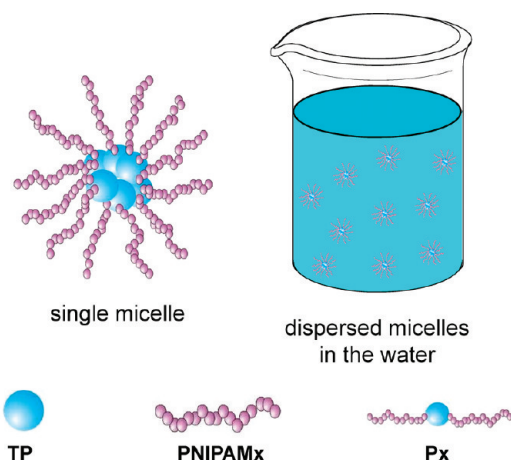
TP content in the aqueous concentration; therefore, the fluorescence signal of the aggregated TPs is directly related to the TP molar concentration.

Dynamic light scattering (DLS) was then used to measure the dimensions of the involved micelles in water. Figure 6 shows the size distribution curves of the nanoparticles involved in the dilute (1 mg/mL) solutions of P1, P2, and P3 at room temperature. Clearly, the average hydrodynamic diameter (D_hs) of the

involved nanoparticles increases with the molecular weight of the polymer; that is, P3 has the highest D_h value of 43 nm in comparison to 28 nm for P2 and 22 nm for P3. Comparative experiment on the PNIPAM1 solution resulted in no detectable DLS signal; therefore, formation of nanoparticles in the Px solutions is due to the small amounts of the hydrophobic TP core embedded in the hydrophilic PNIPAM chain segments. Presumably, the nanoassemblies referred here are micelles with TP core surrounded by the extended PNIPAM segments served as the coronas (cf. the micellar structure in Scheme 2). The preferable π—π interactions of the phenyl rotors of the TP fluorophores are the driving forces contributing to the formation of nanoaggregates of multiple-polymer chains.

Cryo-TEM was applied to examine the actual morphologies of the TP-containing Px nanoparticles in the dilute aqueous solution with the same concentration of 1 mg/mL. The cryo-TEM image of the aqueous P1 solution in Figure 6B revealed the presence of spherical nanoparticles with diameters in the range of 18 —27 nm. The results are in reasonable agreement with that determined by DLS (Figure 6A). The cryo-TEM images of P2 and P3 polymers (Figure S9A and 9B, Supporting Information) are also consistent with the DLS results with the detected particles' diameters in the ranges 23—34 and 33—51 nm, respectively. The observed dimensions are basically dependent on the molecular weights of the Px samples.

Temperature-Programming Self-Assembly of TP-Embedded PNIPAMs. As suggested above, TP-embedded PNIPAMs formed core—shell micelles in water at room temperature. By heating to temperature above LCST, the originally extended hydrophilic PNIPAM chains were converted to a more hydrophobic
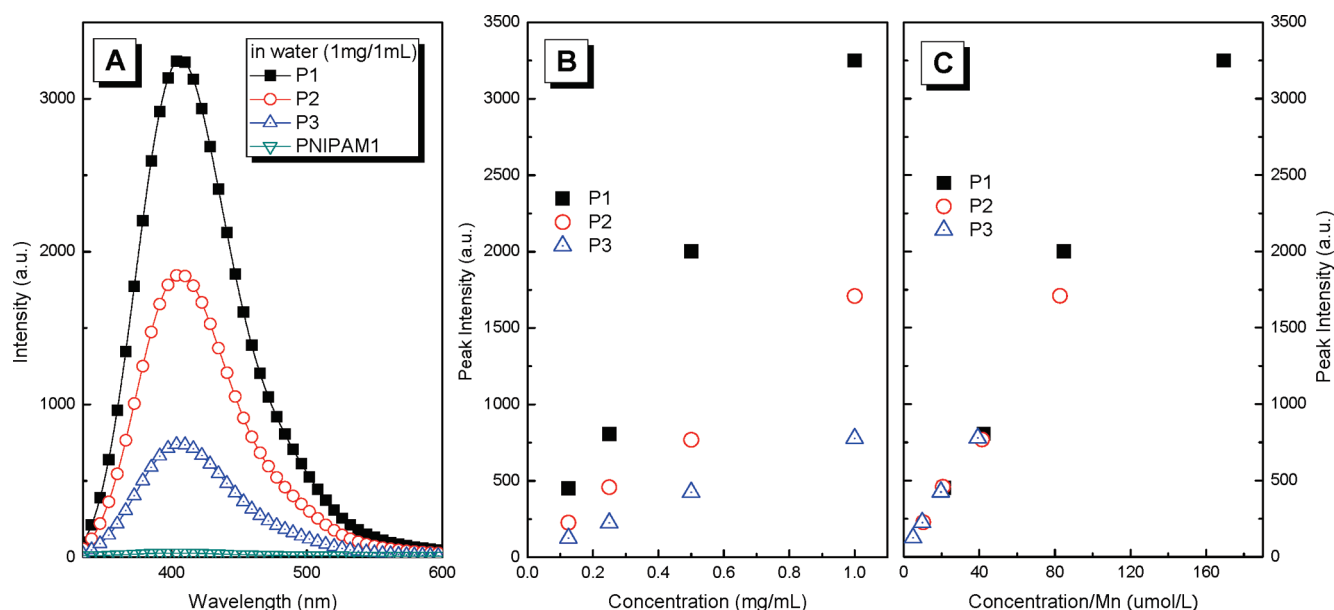
Figure 5. (A) FL emission spectra of aqueous solutions of polymers P1−P3. Concentration of Px: 1 mg/mL. Temperature: 25 °C. Excitation wavelength: 320 nm. (B) FL emission intensities of P1−P3 at 405 nm vs solution concentration and (C) plot of peak intensity as a function of the TP concentration in umol/L from (B). Temperature: 25 °C. Excitation wavelength: 320 nm.
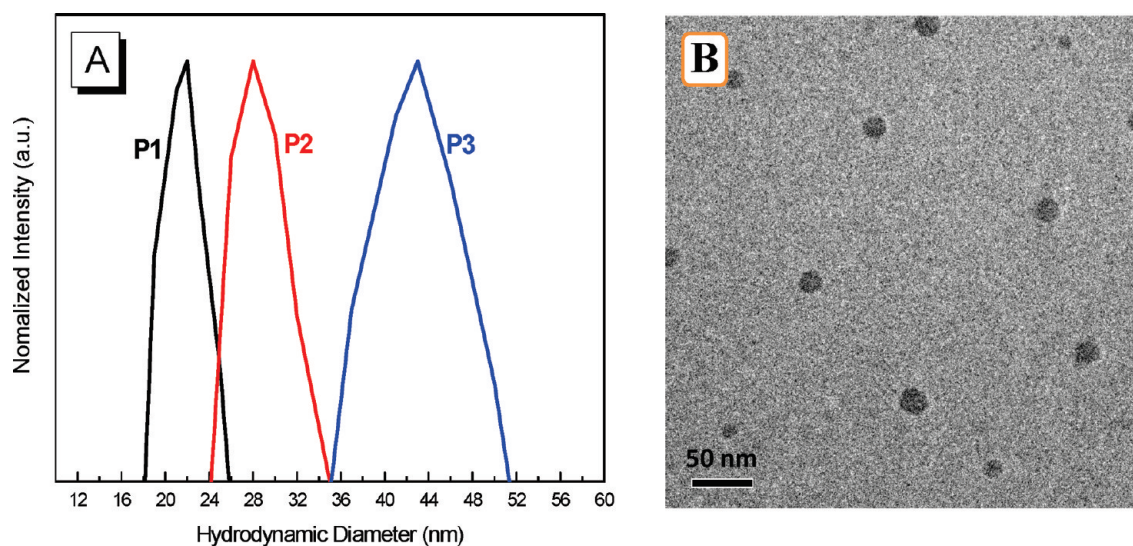
Figure 6. (A) Histograms of hydrodynamic diameters of P1, P2, and P3 (1 mg/mL) in water and (B) cryo-TEM image of micellar structure of P1 in water.

chain state due to the dissociation of hydrogen-bonds and further aggregation should proceed with the reduced hydrophilicity of the polymer chains. At elevated temperatures above the LCST of PNIPAM, the originally formed micelles should undergo structural transformations due to the collapse/aggregation of the PNIPAM segments. The varied responses of the hydrophobic TP core and the hydrophilic PNIPAM shell at high temperatures should affect the resultant FL emission behavior and are the subject to be discussed below. The thermoresponsive behavior of the aqueous Px solutions can be investigated by the combined instrumentations including temperature-dependent FL emission spectra, optical transmittance, DLS, and ^{1}H NMR spectroscopy.

Aqueous solution of P1 is transparent at room temperature (left, Figure 7A) but becomes highly opaque (right, Figure 7A) when heated to 40 °C. This visual difference can be reversibly manipulated by heating and cooling cycle. The variations of solution transparency with temperature can be traced by transmittance measurement. Here, optical transmittance at 700 nm is beyond both the absorption and the emission ranges of the TP fluorophore and was used to locate LCST without the possible interference by the UV−vis absorption and the FL emission from the TP core. The temperature-dependent optical transmittance of the aqueous P1 solution was used as representative to correlate with the average hydrodynamic diameter (D_h) measured in the same temperature ranges (Figure 7B). The resultant transmittance
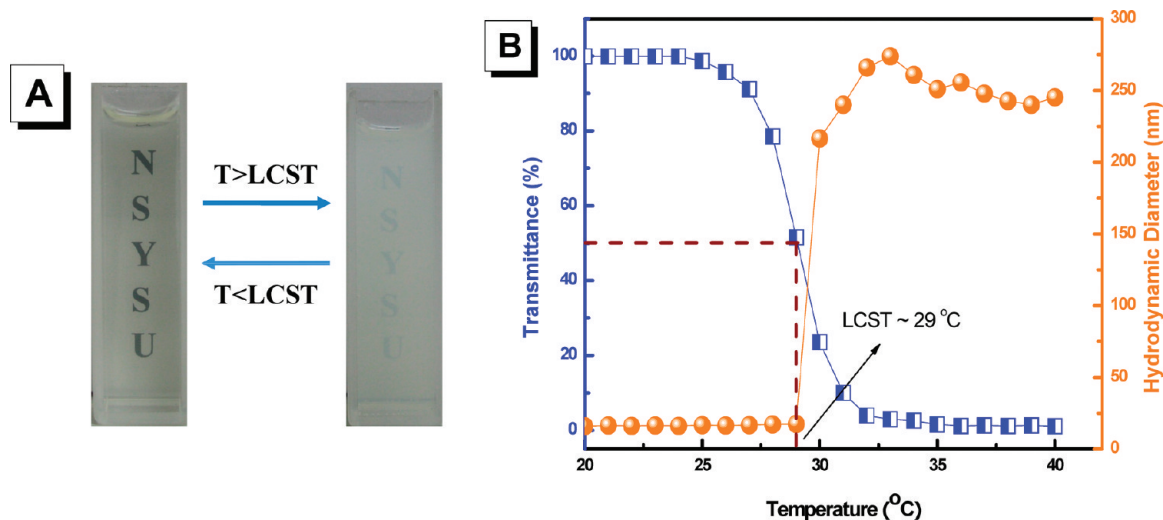
Figure 7. (A) Photograph showing an aqueous solution of P1 at room temperature (left) and at 40 °C (right) and (B) transmittance (blue line + symbol) and hydrodynamic diameter (orange line + symbol) vs temperature for the aqueous P1 (1 mg/mL) solution (monitored at 700 nm).

decreased when heated to above 28 °C and became nil at >32 °C. The sudden transmittance drop in the temperature ranges of 28 and 32 °C indicates that further aggregations of the originally formed micelles proceeded, forming large nanoparticles capable to scatter incident light to result in opaqueness of the solutions at high temperatures. The self-assembled aggregations above LCST was evidenced by the corresponding D_hs measured in the same temperature ranges: the resolved D_hs are quiet constant (∼22 nm) below 29 °C but beyond that, the corresponding D_hs increase drastically to the highest value of 275 nm at 33 °C before reaching the constant value of 250 nm at 40 °C. The high D_hs (>250 nm) detected above LCST are essentially different from the micelle dimensions (∼22 nm) observed below LCST. The initial micelles formed at low temperatures therefore underwent further aggregation to form large entities when heated.

Optical transmittance and DLS were also conducted on the aqueous P2 and P3 (Figure S10A and 10B, Supporting Information) solutions in the same temperature ranges. Both of the P2 and the P3 solutions exhibited the same responses toward temperatures as the P1 solution behaved. The LCSTs thus located by transmittance measurement are 29 °C for P1, 30.1 °C for P2, and 31.3 °C for P3, respectively. The introduction of hydrophobic TP central groups should lower the miscibility of the polymer in water as a result of unfavorable interactions between water and the hydrophobic TP center. In addition, the mixing entropy of the polymer chains is reduced due to the increase of the apparent molecular weight with the introduction of TP core. Both factors favor phase separation, so that the resolved LCSTs tend to shift downward. The factors leading to the early phase separation are larger in polymer with higher hydrophobicity, which was reflected in the observed lower LCST of the P1 polymer as compared to P2 (or P3) polymer with lower hydrophobicity.

Emission of the AIE-active TP core in P*x* is considered to correlate with the extent of aggregation in the nanoparticles formed in the solutions. Therefore, the temperature-programming emission study should provide valuable information on the structural variations during heating. The maximum emission peak intensity of P1, P2 and P3 solutions at 405 nm was measured at varied temperatures from 20 to 43 °C and the results

were summarized in Figure 8A. The initial emission intensity resolved here follows the order of P1 > P2 > P3, which is consistent with the degree of TP-labeling in all three polymers. When heated between 20 to 29 °C, the aqueous P1 solution emitted with constant intensity; however, further heating beyond 29 °C resulted in the sudden emission slump until the complete emission quench at 34.4 °C. Similar responses were observed for the aqueous P2 and P3 solutions. The apparent emission reductions were also observed for the aqueous P2 and P3 solutions. The large emission reduction should be correlated with the self-assembly aggregation process at temperatures above LCST and can be further verified by the transmittance measurements below.

Since the maximum absorbance of the polymer solutions is located at 320 nm (cf. Figure 3), the optical transmittance at 320 nm was monitored in order to find out the plausible reason for the emission quench at high temperatures. The resultant transmittances of P1, P2, and P3 measured in between 20 to 40 °C were summarized in Figure 8B. As expected, the initial optical transmittance at 20 °C follows the same order of P3 > P2 > P1, which is consistent with the TP content in the polymers and suggests that the TP-core is the real absorber for the 320 nm light. When heated above 30 °C, the transmittance slumped abruptly and reached almost zero before 34 °C. The apparent reduction on the transmittance at 320 nm is due to the onset of efficient Mie scattering caused by the large aggregates formed at high temperatures. As suggested by Figure 7B (and Figure S10), further aggregation of the originally formed micelles resulted in large aggregates with the average D_hs > 250 nm, which happen to be the effective dimensions capable to cause serious Mie scattering on the incident 320 nm light.

To collect more information about chain conformation of P*x* and to gain more insight into the thermal transitions, the ¹H NMR spectra are measured in solvents of different affinities and at different temperatures. When in good solvent of CD₂Cl₂, the ¹H NMR spectrum (Figure 9A) of P1 polymer contains resonance signals of all the protons in the TP fluorophore and the PNIPAM chain. In contrast, we failed to observe the aromatic proton (as H$_j$s) signals of the TP unit of P1 in D₂O (Figure 9B). In D₂O, the hydrophobic TP moieties self-assemble to constitute
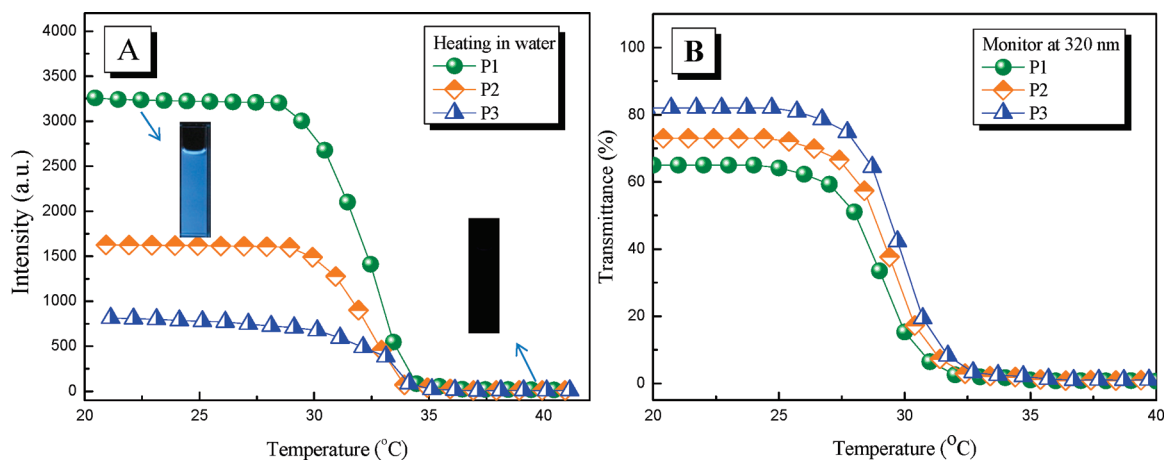
Figure 8. Effects of temperature on (A) the FL emission intensity (excitation wavelength =320 nm) and (B) the optical transmittance of the aqueous P1, P2 and P3 (1 mg/mL) solutions (monitored at 320 nm).
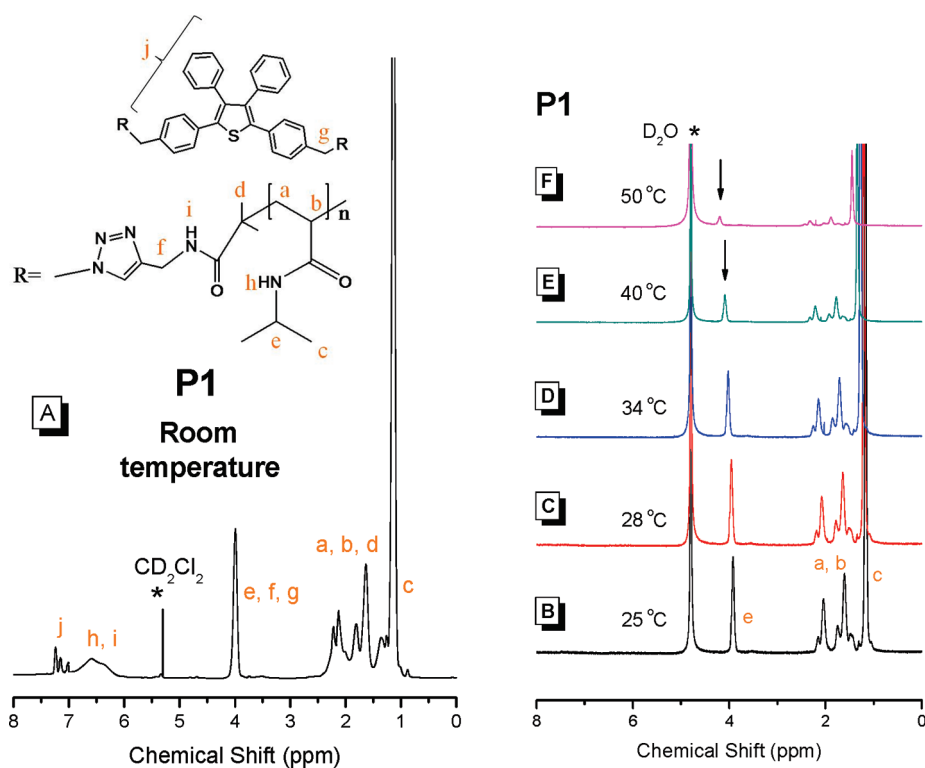
Figure 9. ^{1}H NMR spectra of P1 in (A) CD$_2$Cl$_2$ at 25 °C and (B−F) in D$_2$O at various temperatures.

the central cores of the micelles. The molecular motions of the TP units in the aggregated core are so restricted that their motions can no longer be detected by the ^{1}H NMR in this case. The congested environment in the aggregated core deactivates nonradiative decay channels leading to energy loss, which explains the observed strong FL emission for the dilute aqueous P1 solution (Figure 5A).

In the temperature ranges of 28 and 34 °C, dissociations of hydrogen-bond interactions result in dehydration and the following phase separation to form compact aggregates, which can be detected by the ^{1}H NMR spectra recorded at temperatures above LCST (Figure 9B−F). At high temperatures, the molecular motions of the PNIPAM chains and the TP fluorophores

within the large nanaparticles are supposed to be largely restricted. As indicated by Figure 9B−F, the molecular rotations of the main (protons H$_a$ and H$_b$) and the side (protons H$_e$) chain segments of the PNIPAM are so highly hampered that they gradually lost the resonance resolutions with increasing temperatures. Same experimental results were observed in the temperature-programming ^{1}H NMR spectra (Figure S11, Supporting Information) of P2 and P3 in D$_2$O. Again, we failed to observe the aromatic proton signals in the high temperature ranges. At high temperature, PNIPAM is not soluble in water and it interacts more strongly with itself and the TP unit, resulting in a breakup of the TP aggregates. The TP unit was attached to PNIPAM segment whose motion was strongly

restricted, therefore, the motion of the isolated TPs was also restricted and their signal was not seen by the ^{1}H NMR. The molecular motions of the PNIPAM and the TP units are highly restricted; however, the breakup of the TP aggregates resulted in the disappearance of the AIE-oriented emission at high temperature.

CONCLUSIONS

Thermoresponsive water-soluble PNIPAMs containing single AIE-active TP center were prepared via the combination of atom transfer radical polymerization (ATRP) and click chemistry. Alkynyl-terminated PNIPAMx and diazide-functinalized TPN$_3$ precursor were prepared first. The target polymers Px were then obtained via the click reaction of the alkynyl-terminated PNI-PAMx and the TPN$_3$ precursor. Primary evaluation indicates that the FL emission intensity of the Px in water is linearly proportional to the TP content (cf. Figure 5C). Therefore, the FL signal of the aggregated TPs in the single macromolecular micelles is directly related to the TP molar concentration.

The resultant Px exhibited AIE-characters with enhanced emission in THF/hexane mixtures. Supramolecualr self-assembly in aqueous solutions resulted in the micellar nanoparticles, which undergo subsequent structural transformation during the LCST. The resultant LCST locates at higher temperatures for Px with higher TP-labeling. All the novel AIE-active Px polymers exhibited thermoresponsive FL emission. Complete emission quench occurred when aqueous solutions were heated at temperature above LCST. At low temperature, the aggregated TP fluorophores in the micellar structures exerted the AIE-oriented emissions; however, heating to temperature higher than LCST resulted in the dissociations of the TP aggregates and the emission quench.

ASSOCIATED CONTENT

ⓢ Supporting Information. All supporting data including the sample characterizations (^{1}H NMR, FTIR spectra, DSC thermogram), calibration curve, cryo-TEM images, DLS, transmittance measurements and temperature-programming ^{1}H NMR spectra of P2 and P3 polymers. This material is available free of charge via the Internet at http://pubs.acs.org/.

AUTHOR INFORMATION

Corresponding Author
*E-mail: jlhong@mail.nsysu.edu.tw. Telephone: +886-7-5252000 ext4065.

ACKNOWLEDGMENT

REFERENCES

(1) Schild, H. G. *Prog. Polym. Sci.* **1992**, *17*, 163–249.
(2) Inomata, H.; Goto, S.; Saito, S. *Macromolecules* **1990**, *23*, 4887–4888.
(3) Rzaev, Z. M. O.; Dincer, S.; Piskin, E. *Prog. Polym. Sci.* **2007**, *32*, 534–595.
(4) Tam, K. C.; Wu, X. Y.; Pelton, R. H. *J. Polym. Sci., Polym. Chem. Ed.* **1993**, *31*, 963–969.

(5) Tiktopulo, E. I.; Bychkova, V. E.; Ricka, J.; Ptitsyn, O. B. *Macromolecules* **1994**, *27*, 2879–2882.
(6) Wang, X.; Qiu, X.; Wu, C. *Macromolecules* **1998**, *31*, 2972–2976.
(7) Maeda, Y.; Higuchi, T.; Ikeda, I. *Langmuir* **2001**, *17*, 7535–7539.
(8) Stieger, M.; Richtering, W. *Macromolecules* **2003**, *36*, 8811–8818.
(9) Kita, R.; Wiegand, S. *Macromolecules* **2005**, *38*, 4554–4556.
(10) Ye, J.; Xu, J.; Hu, J.; Wang, X.; Zhang, G.; Liu, S.; Wu, C. *Macromolecules* **2008**, *41*, 4416–4422.
(11) Zhou, K.; Lu, Y.; Li, J.; Shen, L.; Zhang, G.; Xie, Z.; Wu, C. *Macromolecules* **2008**, *41*, 8927–8931.
(12) Ye, X.; Lu, Y.; Shen, L.; Ding, Y.; Liu, S.; Zhang, G.; Wu, C. *Macromolecules* **2007**, *40*, 4750–4752.
(13) Matsuyama, A.; Tanaka, F. *J. Chem. Phys.* **1991**, *94*, 781–786.
(14) Wu, C.; Zhou, S. *Macromolecules* **1995**, *28*, 5388–5390.
(15) Okada, Y.; Tanaka, F. *Macromolecules* **2005**, *38*, 4465–4471.
(16) Taylor, L. D.; Cerankowski, L. D. *J. Polym. Sci., Polym. Chem. Ed.* **1975**, *13*, 2551–2570.
(17) Kikuchi, A.; Okano, T. *Adv. Drug Delivery Rev.* **2002**, *54*, 53–77.
(18) Gil, E. S.; Hudson, S. M. *Prog. Polym. Sci.* **2004**, *29*, 1173–1222.
(19) Schild, H. G.; Tirrell, D. A. *Langmuir* **1991**, *7*, 1319–1324.
(20) Ringsdorf, H.; Venzmer, J.; Winnik, F. M. *Macromolecules* **1991**, *24*, 1678–1686.
(21) Chung, J. E.; Yokoyama, M.; Suzuki, K.; Aoyagi, T.; Sakurai, Y.; Okano, T. *Colloids Surf. B* **1997**, *9*, 37–48.
(22) Chung, J. E.; Yokoyama, M.; Aoyagi, T.; Sakurai, Y.; Okano, T. *J. Controlled Release* **1998**, *53*, 119–130.
(23) Zhang, Y. B.; Li, M.; Fang, Q.; Zhang, Y. X.; Jiang, M.; Wu, C. *Macromolecules* **1998**, *31*, 2527–2532.
(24) Cao, Z.; Liu, W.; Gao, P.; Yao, K.; Li, H.; Wang, G. *Polymer* **2005**, *46*, 5268–5277.
(25) Winnik, F. M.; Davidson, A. R.; Hamer, G. K.; Kitano, H. *Macromolecules* **1992**, *25*, 1876–1880.
(26) Winnik, M. A.; Yekta, A. *Curr. Opin. Colloid Interface Sci.* **1997**, *2*, 424–436.
(27) Pham, Q. T.; Russel, W. B.; Thibeault, J. C.; Lau, W. *Macromolecules* **1999**, *32*, 2996–3005.
(28) Beaudoin, E.; Borisov, O.; Lapp, A.; Billon, L.; Hiorns, R. C.; Francois, J. *Macromolecules* **2002**, *35*, 7436–7447.
(29) Kujawa, P.; Watanabe, H.; Tanaka, F.; Winnik, F. M. *Eur. Phys. J. E* **2005**, *17*, 129–137.
(30) Li, C.; Hu, J.; Yin, J.; Liu, S. *Macromolecules* **2009**, *42*, 5007–5016.
(31) Zhou, G.; Harruna, I. I.; Zhou, W. L.; Aicher, W. K.; Geckeler, K. E. *Chem.—Eur. J.* **2007**, *13*, 569–573.
(32) Tamura, A.; Uchida, K.; Yajima, H. *Chem. Lett.* **2006**, *35*, 282–283.
(33) Xie, J. Z.; Lam, J. W. Y.; Cheng, L.; Chen, H.; Qiu, C.; Kwok, H. S.; Zhan, X.; Liu, Y.; Zhu, D.; Tang, B. Z. *Chem. Commun.* **2001**, 1740–1741.
(34) Dong, S.; Li, Z.; Qin, J. *J. Phys. Chem. B* **2009**, *113*, 434–441.
(35) Yuan, C. X.; Tao, X. T.; Wang, L.; Yang, J. X.; Jiang, M. H. *J. Phys. Chem. C* **2009**, *113*, 6809–6814.
(36) Liu, Y.; Tao, X.; Wang, F.; Dang, X.; Zou, D.; Ren, Y.; Jiang, M. *J. Phys. Chem. C* **2008**, *112*, 3975–3981.
(37) Qian, L.; Tong, B.; Shen, J.; Shi, J.; Zhi, J.; Dong, Y.; Yang, F.; Dong, Y.; Lam, J. W. Y.; Liu, Y.; Tang, B. Z. *J. Phys. Chem. B* **2009**, *113*, 9098–9103.
(38) Yang, Z.; Chi, Z.; Yu, T.; Zhang, X.; Chen, M.; Xu, B.; Liu, S.; Zhang, Y.; Xu, J. *J. Mater. Chem.* **2009**, *19*, 5541–5546.
(39) Yuan, W. Z.; Lu, P.; Chen, S.; Lam, J. W. Y.; Wang, Z.; Liu, Y.; Kwok, H. S.; Ma, Y.; Tang, B. Z. *Adv. Mater.* **2010**, *22*, 1–5.
(40) Xu, B.; Chi, Z.; Yang, Z.; Chen, J.; Deng, S.; Li, H.; Li, X.; Zhang, Y.; Xu, N.; Xu, J. *J. Mater. Chem.* **2010**, *20*, 4135–4141.
(41) Zhao, Z.; Chen, S.; Lam, J. W. Y.; Jim, C. K. W.; Chan, C. Y. K.; Wang, Z.; Lu, P.; Deng, C.; Kwok, H. S.; Ma, Y.; Tang, B. Z. *J. Phys. Chem. C* **2010**, *114*, 7963–7972.
(42) Zhao, Z.; Chen, S.; Lam, J. W. Y.; Lu, P.; Zhong, Y.; Wong, K. S.; Kwok, H. S.; Tang, B. Z. *Chem. Commun.* **2010**, *46*, 2221–2223.

(43) Wang, W.; Lin, T.; Wang, M.; Liu, T. X.; Ren, L.; Chen, D.; Huang, S. *J. Phys. Chem. B* **2010**, *114*, 5983–5988.

(44) Kokado, K.; Chujo, Y. *Macromolecules* **2009**, *42*, 1418–1420.

(45) Tang, L.; Jin, J. K.; Qin, A.; Yuan, W. Z.; Mao, Y.; Mei, J.; Sun, J. Z.; Tang, B. Z. *Chem. Commun.* **2009**, 4974–4976.

(46) Liu, J.; Lam, J. W. Y.; Tang, B. Z. *J. Inorg. Organomet. Polym.* **2009**, *19*, 249–285.

(47) Lai, C. T.; Hong, J. L. *J. Phys. Chem. C* **2009**, *113*, 18578–18583.

(48) Liu, J.; Zhong, Y.; Lam, J. W. Y.; Lu, P.; Hong, Y.; Yu, Y.; Yue, Y.; Faisal, M.; Sung, H. H. Y.; Williams, I. D.; Wong, K. S.; Tang, B. Z. *Macromolecules* **2010**, *43*, 4921–4936.

(49) Qin, A.; Lam, J. W. Y.; Tang, L.; Jim, C. K. W.; Zhao, H.; Sun, J.; Tang, B. Z. *Macromolecules* **2009**, *42*, 1421–1424.

(50) Chien, R. H.; Lai, C. T.; Hong, J. L. *J. Phys. Chem. C* **2011**, *115*, 5958–5965.

(51) Lai, C. T.; Hong, J. L. *J. Phys. Chem. B* **2010**, *114*, 10302–10310.

(52) Chou, C. A.; Chien, R. H.; Lai, C. T.; Hong, J. L. *Chem. Phys. Lett.* **2010**, *501*, 80–86.

(53) Imai, Y.; Maldar, N. N.; Kakimoto, M. *J. Polym. Sci., Polym. Chem. Ed.* **1984**, *22*, 2189–2196.

(54) Su, F. K.; Hong, J. L.; Lin, L. L. *Synth. Met.* **2004**, *142*, 63–69.

(55) Yang, C. H.; Lin, L. L.; Hong, J. L. *Polym. Int.* **2005**, *54*, 679–685.

(56) Inceoglu, S.; Olugebefola, S. C.; Acar, M. H.; Mayes, A. M. *Des. Monomers Polym.* **2004**, *7*, 181–189.

(57) Adrian, M.; Dubochet, J.; Lepault, J.; McDowall, A. W. *Nature* **1984**, *308*, 32–36.

(58) Dubochet, J.; Adrian, M.; Chang, J. J.; Homo, J.-C.; Lepault, J.; McDowall, A. W.; Schultz, P. *Quart. Rev. Phys.* **1988**, *21*, 129–228.

(59) Rostovtsev, V. V.; Green, L. G.; Fokin, V. V.; Sharpless, K. B. *Angew. Chem., Int. Ed.* **2002**, *41*, 2596–2599.

(60) Tornoe, C. W.; Christensen, C.; Meldal, M. *J. Org. Chem.* **2002**, *67*, 3057–3064.